Renal histopathological analysis of 26 postmortem findings of patients with COVID-19 in China

Hua Su[1,5], Ming Yang[2,5], Cheng Wan[1], Li-Xia Yi[1], Fang Tang[1], Hong-Yan Zhu[1], Fan Yi[3], Hai-Chun Yang[4], Agnes B. Fogo[4], Xiu Nie[2] and Chun Zhang[1]

OPEN

[1]Department of Nephrology, Union Hospital, Tongji Medical College, Huazhong University of Science and Technology, Wuhan, China; [2]Department of Pathology, Union Hospital, Tongji Medical College, Huazhong University of Science and Technology, Wuhan, China; [3]The Key Laboratory of Infection and Immunity of Shandong Province, Department of Pharmacology, School of Basic Medical Sciences, Shandong University, Jinan, China; and [4]Department of Pathology, Microbiology and Immunology, Vanderbilt University Medical Center, Nashville, Tennessee, USA

Although the respiratory and immune systems are the major targets of Coronavirus Disease 2019 (COVID-19), acute kidney injury and proteinuria have also been observed. Currently, detailed pathologic examination of kidney damage in critically ill patients with COVID-19 has been lacking. To help define this we analyzed kidney abnormalities in 26 autopsies of patients with COVID-19 by light microscopy, ultrastructural observation and immunostaining. Patients were on average 69 years (19 male and 7 female) with respiratory failure associated with multiple organ dysfunction syndrome as the cause of death. Nine of the 26 showed clinical signs of kidney injury that included increased serum creatinine and/or new-onset proteinuria. By light microscopy, diffuse proximal tubule injury with the loss of brush border, non-isometric vacuolar degeneration, and even frank necrosis was observed. Occasional hemosiderin granules and pigmented casts were identified. There were prominent erythrocyte aggregates obstructing the lumen of capillaries without platelet or fibrinoid material. Evidence of vasculitis, interstitial inflammation or hemorrhage was absent. Electron microscopic examination showed clusters of coronavirus particles with distinctive spikes in the tubular epithelium and podocytes. Furthermore, the receptor of SARS-CoV-2, ACE2 was found to be upregulated in patients with COVID-19, and immunostaining with SARS-CoV nucleoprotein antibody was positive in tubules. In addition to the direct virulence of SARS-CoV-2, factors contributing to acute kidney injury included systemic hypoxia, abnormal coagulation, and possible drug or hyperventilation-relevant rhabdomyolysis. Thus, our studies provide direct evidence of the invasion of SARSCoV-2 into kidney tissue. These findings will greatly add to the current understanding of SARS-CoV-2 infection.

Correspondence: *Chun Zhang, Department of Nephrology, Union Hospital, Tongji Medical College, Huazhong University of Science and Technology, 1277 Jie Fang Avenue, Wuhan, Hubei 430022, China. E-mail: drzhangchun@hust.edu.cn; or Xiu Nie, Department of Pathology, Union Hospital, Tongji Medical College, Huazhong University of Science and Technology, 1277 Jie Fang Avenue, Wuhan 430022, China. E-mail: niexiuyishi@126.com*

[5]These authors contributed equally to this work.

Received 1 April 2020; revised 5 April 2020; accepted 6 April 2020; published online 9 April 2020

Kidney International (2020) ■, ■–■; https://doi.org/10.1016/j.kint.2020.04.003

KEYWORDS: acute kidney injury; COVID-19; proteinuria; renal pathology; SARS-CoV-2

In December 2019, a cluster of patients with pneumonia of unknown etiology was reported in Wuhan, Hubei Province, China. On January 9, 2020, the Chinese Center for Disease Control and Prevention identified the causative agent as a novel coronavirus, which now is officially termed severe acute respiratory syndrome coronavirus 2 (SARS-CoV-2).[1] The illness caused by SARS-CoV-2, coronavirus disease 2019 (COVID-19), mainly manifests with fever, dry cough, dyspnea, myalgia, and diarrhea. However, COVID-19 presentations can range from asymptomatic infection, self-limited influenza-type symptoms, and acute pneumonia to severe respiratory failure with high mortality. Currently, the epidemic in China is being gradually controlled with major domestic efforts and international support. However, the global epidemic has now become a pandemic.

Without knowing the detailed mechanisms of COVID-19, specific management is lacking. The reported mortality in different countries varies according to extent of testing performed, ranging from 0.3% to 10%. The respiratory, immune, and coagulation systems are the major targets of this pandemic disease.[2] Kidney injury has appeared relatively less with COVID-19 than with Middle East respiratory syndrome or hantavirus infections, perhaps due to the different underlying mechanisms and ensuing pathologic manifestations. Clinically, the incidence of acute kidney injury (AKI) in COVID-19 varied from 0.9% to 29% in different centers. New onset proteinuria was also reported by several institutions.[3] Currently, the pathologic investigation has primarily focused on respiratory, hematopoietic, and immune systems, whereas morphologic data of kidney injury are lacking. In this study, we report on our experience of kidney findings at autopsy in patients with severe COVID-19.

RESULTS

Clinical information

The 26 patients with COVID-19 included 19 males and 7 females, with an average age of 69 years (range, 39–87 years). All 26 cases had positive results for SARS-CoV-2 by nucleic acid testing and characteristic radiologic alterations in lungs. Eleven patients had history of hypertension or diabetes or both. Data on angiotensin-converting enzyme (ACE) inhibitors or angiotensin-receptor blockers for hypertension or diabetes or both before the terminal hospitalization were not available. Patients were treated with calcium-channel blockers if needed for hypertension during the terminal hospitalization, without ACE inhibitors or angiotensin-receptor blockers or both, due to uncertainty regarding possible effects. Six patients had history of tumor. The clinical information is summarized in Tables 1 and 2.

Light microscopy findings

All tissue samples were well preserved without autolysis. There was prominent proximal acute tubule injury (ATI) manifested as the loss of brush border, vacuolar degeneration, dilatation of the tubular lumen with cellular debris, and occasionally even frank necrosis and detachment of epithelium with bare tubular basement membrane noted (the latter observed in 4 cases). The majority of the vacuoles in cytoplasm were variable in size; however, focal isometric fine vacuolization was uncommonly present and is associated with, for example, mannitol or i.v. Ig therapy (Figure 1a and b). In 2 patients, consistent with corresponding pathologic findings in their lungs, acute pyelonephritis was observed with multiple foci of bacteria and diffuse polymorphonuclear casts in the lumen of tubules. In 1 of these 2 patients, an arcuate artery was infiltrated with numerous inflammatory cells (Figure 1c and d), likely representing reaction to bacterial infection. Diffuse erythrocyte aggregation and obstruction were present in peritubular and glomerular capillary loops without distinct fragmentation of erythrocytes or platelets or fibrin thrombi.

Occasional hemosiderin granules in tubular epithelium were identified in 4 patients with hematuria by dipstick (Figure 1e). In 3 cases, pigmented casts were found with high levels of creatine phosphokinase, possibly representing rhabdomyolysis (Figure 1f). Distal tubules and collecting ducts showed only occasional cellular swelling and edematous expansion of the interstitial space without significant inflammation. Lymphocytic infiltrates were present in areas of nonspecific fibrosis including subcapsular areas.

Glomeruli showed varied degrees of underlying morphologic changes, such as nodular mesangial expanding and hyalinosis of arterioles, which constituted evidence of diabetic nephropathy in 2 of the patients with diabetes, and arteriosclerosis of medium-size arteries with ischemic glomeruli in 11 of the patients with hypertension. Focal obsolescent glomeruli were detected proportional to the age in this population. Endothelial cell swelling with variable foamy degeneration was present in 5 of the patients with COVID-19, and they were usually older and had hypertensive or diabetic histories. In 3 cases, a few areas of segmental fibrin thrombus in glomerular capillary loops were identified associated with severe injury of the endothelium (Figure 1g). Occasional podocyte vacuolation and even detachment from the glomerular basement membrane was noted. Focal segmental glomerulosclerosis was observed in 2 patients with overt proteinuria as well as history of diabetes. Ischemic changes with shrinkage of capillary loops with accumulation of plasma in Bowman's space was present in 7 cases, occasionally with pseudocrescent appearance (Figure 1h). Crescents and hypercellular or inflammatory lesions of glomeruli were not present. The pathologic findings are summarized in Table 3.

Transmission electron microscopy observations

Virus particles were identified in the cytoplasm of renal proximal tubular epithelium as well as in the podocytes and less so in distal tubules. The diameter of virus particles varied from about 65 nm to 136 nm, with distinctive spikes, around 20 to 25 nm, presenting in a solar "corona" appearance. Additional features of this coronavirus included adjacent double membrane with surface projections, nucleocapsid apposing to the viral envelope, and the interior electron-lucent of the particles (Figure 2a–d).

In 1 case, paramesangial and subendothelial deposits with segmental mesangial interposition and increased lamina rara interna were present (Figure 2e); and scattered subepithelial "hump-like" deposits were noted in another case. No other diagnostic electron-dense deposits were detected. These 2 patients did not have evidence of bacterial infection at autopsy in lungs or kidneys.

In 2 of 3 patients with diabetes, characteristic changes of diabetic nephropathy were present by electron microscopy (EM), including increased thickness of the glomerular basement membrane without deposits, mesangial expansion and segmental foot process effacement, and microvillous transformation.

Abundant erythrocytes were observed obstructing peritubular capillary lumens with activation of endothelium (Figure 2f). Platelet aggregations or fibrin tactoids were not detected in association with this lesion. Aggregation of erythrocytes in segmental glomerular capillary loops was frequent, without inflammation or necrosis. In patent glomerular capillary loops, a varied extent of endothelial injury was noted, including swelling, foamy-like change, subendothelial lucent expansion, and endothelial proliferation without deposits. The ultrastructural findings are summarized in Table 3.

Immunostaining findings

Immunohistochemical (IHC) staining for various inflammatory cells did not show any specific accumulation of these cells, with expected mix of T and B cells in areas of nonspecific scarring with lymphocytic infiltrate and scattered

Table 1 | Clinical information of 26 patients with COVID-19

ID	Sex	Age (y)	History of HT, DM, CKD or tumor	Hypotension/ vasopressor	BUN (mmol/l)	Cr (μmol/l)	Urine			Hb (g/l)	WBC (g/l)	LY (g/l)	LY%	PLT (T/l)	D-dimer (μg/ml)	ALT (U/l)	AST (U/l)	TBIL (μmol/l)	CK (U/l)
							PRO	BLD	WBC										
1	M	77	N	Y	22.52	239.8	N/A	N/A	N/A	N/A	25.1	0.37	1.50	33	>8.00	60	71	N/A	N/A
2	F	60	N	N	N/A	N/A	−	2+	1+	112	17.87	0.82	4.60	103	2.35	N/A	N/A	N/A	N/A
3	M	51	Pancreas Ca	Y	18.96	71.3	Trace	−	−	96	31.87	0.75	2.40	38	5.61	102	126	110.2	328
4	M	87	DM, HT, CKD	Y	42.45	229.8	N/A	N/A	N/A	70	13.63	0.26	1.90	219	1.08	13	16	9.5	99
5	M	39	Gastric Ca	N	7.18	31	N/A	N/A	N/A	98	11.4	0.44	3.90	273	6.1	15	18	23.9	87
6	M	66	Liver Ca	Y	41.84	161.4	N/A	N/A	N/A	89	12.52	0.24	1.90	57	0.9	184	150	49.1	1001
7	M	77	Skin Ca	Y	24.14	460.2	N/A	N/A	N/A	93	23.59	0.81	3.40	105	5.32	21	48	13.6	312
8	F	87	DM, HT, CKD	Y	N/A	N/A	3+	3+	1+	101	8.98	0.48	5.40	110	>8.00	N/A	N/A	N/A	N/A
9	M	70	Lung Ca	N	12.86	207.3	N/A	N/A	N/A	112	5.76	0.81	14.10	215	2.85	367	840	14.9	2459
10	F	84	HT	N	14.28	114.7	N/A	N/A	N/A	60	7.69	0.53	6.80	75	2.86	29	30	16.1	54
11	F	83	HT	Y	21.54	108	N/A	N/A	N/A	69	2.28	0.17	7.30	30	2.08	717	954	6.5	495
12	M	63	HT	Y	7.3	45.9	−	±	−	102	41.48	0.53	1.30	179	1.02	107	44	8.5	158
13	M	52	N	Y	7.51	58.7	2+	−	±	73	11.19	0.66	5.90	342	2.69	97	52	18.9	194
14	M	61	HT	Y	13.99	94.2	1+	1+	±	80	15.67	0.64	4.10	80	2.3	88	77	41.3	259
15	F	70	HT, Lung Ca	Y	5.79	44.1	N/A	N/A	N/A	102	18.89	1.21	6.40	106	>8.00	54	35	26.1	37
16	M	64	HT	Y	20.42	137.3	N/A	N/A	N/A	93	3.35	0.56	16.80	23	7.69	21	38	18.9	64
17	M	66	HT	Y	3.24	57.9	2+	3+	1+	81	0.26	0.08	29.90	15	4.95	349	157	3.2	N/A
18	F	62	N	Y	11.86	61.8	N/A	N/A	N/A	88	9.14	0.69	7.60	76	3.42	19	18	14.2	23
19	M	55	DM, HT	Y	9.24	43.7	2+	1+	3+	78	1.28	0.08	6.20	18	2.05	599	1199	57.7	34
20	M	83	N/A	N/A	N/A	N/A	N/A	N/A	N/A	N/A	N/A	N/A	N/A	N/A	N/A	N/A	N/A	N/A	N/A
21	F	86	N/A	N/A	N/A	N/A	N/A	N/A	N/A	N/A	N/A	N/A	N/A	N/A	N/A	N/A	N/A	N/A	N/A
22	M	78	N/A	N/A	N/A	N/A	N/A	N/A	N/A	N/A	N/A	N/A	N/A	N/A	N/A	N/A	N/A	N/A	N/A
23	M	62	N/A	N/A	N/A	N/A	N/A	N/A	N/A	N/A	N/A	N/A	N/A	N/A	N/A	N/A	N/A	N/A	N/A
24	M	51	N/A	N/A	N/A	N/A	N/A	N/A	N/A	N/A	N/A	N/A	N/A	N/A	N/A	N/A	N/A	N/A	N/A
25	M	72	N/A	N/A	N/A	N/A	N/A	N/A	N/A	N/A	N/A	N/A	N/A	N/A	N/A	N/A	N/A	N/A	N/A
26	M	86	HT	Y	4.36	63.6	1+	−	−	97	45.44	0.38	0.80	155	3.77	15	35	24.5	213

ALT, alanine aminotransferase; AST, aspartate aminotransferase; BLD, blood; BUN, blood urea nitrogen; Ca, cancer; CK, creatine kinase; CKD, chronic kidney disease; Cr, creatinine; DM, diabetes; F, female; Hb, hemoglobin; HT, hypertension; ID, identification number; LY, lymphocytes; M, male; N, no; N/A, not available; PLT, platelet; PRO, proteinuria; TBIL, total bilirubin; WBC, white blood cell; Y, yes.
The cause of death in all patients was respiratory failure. In addition, patients 1, 5, 14, 15, 16, 25, and 26 had multiorgan failure.

Table 2 | Treatment history

ID	Exposure to nephrotoxic drug	Renal replacement therapy	Antivirals	Steroid
1	N	N	Arbidol	Y
2	Y	CRRT	Arbidol	Y
3	N	N	Ribavirin	N
4	N	N	Ribavirin, arbidol	N
5	N	N	Arbidol	Y
6	N	N	Arbidol	Y
7	N	CRRT	Arbidol	Y
8	N	N	Arbidol	N
9	N	N	N	N
10	N	CRRT	Arbidol	Y
11	N	N	Arbidol	Y
12	N	N	Arbidol	Y
13	Y	N	Lopinavir/ritonavir	Y
14	Y	N	N	Y
15	N	N	Lopinavir/ritonavir	Y
16	N	N	Lopinavir/ritonavir	Y
17	Y	N	N	Y
18	N	CRRT	N	Y
19	N	CRRT	Lopinavir/ritonavir	Y
20	N/A	N/A	N/A	N/A
21	N/A	N/A	N/A	N/A
22	N/A	N/A	N/A	N/A
23	N/A	N/A	N/A	N/A
24	N/A	N/A	N/A	N/A
25	N/A	N/A	N/A	N/A
26	N	N	Lopinavir/ritonavir	Y

CRRT, continuous renal replacement therapy; ID, identification number; N, no; N/A, not available; Y, yes.

macrophages. CD235a (glycophorin A, present in erythrocytes) staining confirmed the microvascular obstruction was composed predominantly of erythrocytes. Serial section staining for CD61 (platelet marker) showed minimal staining in the same field, indicating no significant platelet component, and CD31 staining for endothelial cells showed near complete occlusion of peritubular capillary lumens (Figure 3a). In an archival biopsy of a patient who was nondiabetic, nonhypertensive, and without COVID-19, biopsied for proteinuria, weak ACE II (ACE2) staining of proximal tubules without glomerular staining was observed, which is consistent with previous publications. No detectable signal was observed in the kidney vascular compartment (Figure 3b). ACE2 staining was also done in 5 of the patients (nos. 21, 22, 23, 24, 25), revealing altered ACE2 pattern in 3 of these (nos. 21, 22, 25). ACE2 expression was prominent in proximal tubular cells, particularly in areas with severe ATI. In addition, focal strong parietal epithelial cells staining was present, as well as occasional weaker podocyte staining (Figure 3c).

Direct or indirect immunofluorescent (IF) staining was conducted from paraffin blocks in 6 cases, and nonspecific IgM and C3 trapping were present. One biopsy showed segmental granular capillary IgG, however, without diagnostic C3 staining along the capillary wall, but with scattered humps by EM. One case showed IgA staining in mesangial area as well as capillary wall, associated with corresponding mesangial and subendothelial deposits by EM. By an indirect fluorescence method, the expression of SARS-CoV nucleoprotein was analyzed in the same 6 cases, and 3 showed positive granular staining in a nuclear or cytoplasm pattern in tubular epithelium (Figure 3d). Negative and positive controls showed expected reactivity. The immunostaining findings are summarized in Table 3.

DISCUSSION

In the present study, we report the kidney histopathologic, ultrastructural, and immunostaining findings from autopsies of 26 patients who died from respiratory failure due to COVID-19. This is the first report of kidney pathologic presentations in patients with SARS-CoV-2 infection. Our autopsy study demonstrates the range of abnormalities present and the specific kidney cells likely infected with the virus, and thus may provide important information for future clinicopathologic studies in less severely ill patients with COVID-19 infection and kidney injury. We observed significant ATI, the occlusion of microvascular lumens mainly by erythrocytes with ensuing endothelial damage, as well as glomerular and vascular changes indicative of underlying diabetic or hypertensive disease. Some of these findings are in accordance with former mechanisms known for β-coronavirus infection in kidney. We also show findings that suggest distinct mechanisms of this novel coronavirus infection, involving direct kidney parenchyma infection and likely secondary endothelial injury. Thus, these pathologic observations may provide a basis for further understanding of COVID-19.

We observed diffuse acute proximal tubular injury with loss of brush border and nonisometric vacuolation, which may be partially caused by the direct virulence of SARS-CoV-2, demonstrated by our ultrastructural and immunostaining assessment. The tubular cytoplasmic vacuoles were mostly variable in size. However, in a few patients, focal isometric fine vacuolization was present and is likely related to treatment with hypertonic sucrose or other hyperosmolar fluids, such as i.v. Ig or mannitol therapy.

EM demonstrated spherical virus particles characteristic of coronavirus in proximal tubular epithelium. The diameter of the virus particles and the length of spikes were similar to previously identified coronaviruses causing SARS and Middle East respiratory syndrome.[4] Furthermore, virus particles were clearly identified in podocytes, associated with foot process effacement and occasional vacuolation and detachment of podocytes from the glomerular basement membrane. Virus infection was confirmed by IF staining using an antibody targeting SARS-CoV nucleoprotein shared between β-coronaviruses. These findings indicate that SARS-CoV-2 virus can directly infect the renal tubular epithelium and podocytes, which was associated with AKI and proteinuria in these patients with COVID-19.

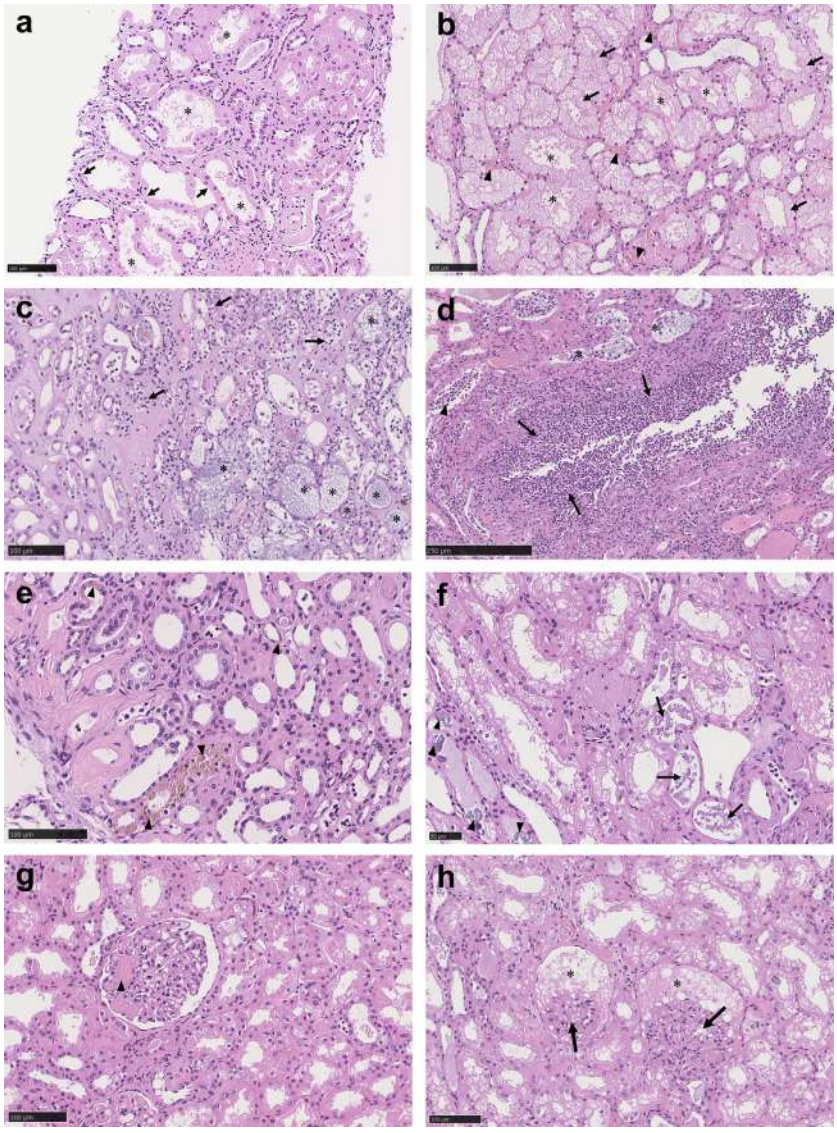

Figure 1 | Spectrum of pathologic abnormalities of kidneys from postmortems of patients with coronavirus disease 2019. (**a,b**) Proximal tubules showed (**a**) loss of brush border and (**b**) vacuolar degeneration (arrows), with debris composed of necrotic epithelium in tubular lumens (asterisks). Erythrocyte aggregates obstructing peritubular capillaries were frequently present (arrowheads). (**c,d**) Some cases showed infiltration of inflammatory cells in (**c**) tubules and (**d**) in 1 case, in an arcuate artery (arrows), with multiple foci of bacteria (asterisks) and white blood cell casts (arrowhead). (**e,f**) Occasional (**e**) hemosiderin granules and (**f**) deposits of calcium (arrowheads) were present in tubules with occasional pigmented casts (arrows). (**g,h**) Segmental fibrin thrombi were present in glomeruli (arrowhead), with ischemic glomerular contraction (arrows) with the accumulation of leaked plasma in Bowman's space (asterisks). Hematoxylin and eosin. Bars = (**f**) 50 μm, (**a–c,e,g,h**) 100 μm, and (**d**) 250 μm. To optimize viewing of this image, please see the online version of this article at www.kidney-international.org.

Another common morphologic finding was erythrocyte stagnation in the lumen of glomerular and peritubular capillaries without platelets, red blood cell fragments, fibrin thrombi, or fibrinoid necrosis. Interestingly, in cases with predominant glomerular loop occlusion, less red blood cell aggregation was present in peritubular capillaries, which is often associated with a relatively long duration of hypotension.

Pigmented casts were present in some patients and were associated with apparent rhabdomyolysis with high serum levels of creatine phosphokinase. Potentially, drug- or hyperventilation-relevant rhabdomyolysis contributed, although a direct viral effect on muscle is also possible. Of note, there was no interstitial hemorrhage as is characteristic for AKI induced by hantavirus infection.[5] Furthermore, diagnostic vasculitis, one of the morphologic features of lung-kidney syndrome caused by anti-neutrophil cytoplasmic antibodies,[6] was not identified in these patients with COVID-19.

SARS-CoV-2 shares 79% homology with SARS-CoV, the causal agent of SARS outbreaks in China 18 years ago.[7] They

Table 3 | The pathologic abnormalities of kidney in 26 cases of deceased patients with COVID-19

	LM						EM			IF		
	Tubule interstitium				Glomeruli							
ID	ATI	Multiple foci of bacteria	Pigmented casts	Arteriosclerosis	Segmental fibrin thrombus	FSGS	Virus particles	Dense deposits	Subendothelial lucent expansion	IgG	IgA	SARS-CoV NP
1	Severe	N	N	Mild to moderate	N	N	N/A	N/A	N/A	N/A	N/A	N/A
2	Moderate	N	N	Mild	N	N	Y	N	N	N/A	N/A	N/A
3	Mild to moderate	N	Y	Mild	N	N	Y	N	Y	N/A	N/A	N/A
4	Severe	N	N	Severe	N	Y	Y	N	Y	N/A	N/A	N/A
5	Mild	N	N	Mild	N	N	N/A	N/A	N/A	N/A	N/A	N/A
6	Mild to moderate	N	Y	Mild	N	N	N/A	N/A	N/A	N/A	N/A	N/A
7	Severe	N	N	Mild to moderate	N	N	N/A	N/A	N/A	N/A	N/A	N/A
8	Moderate	N	N	Severe	Focal	Y	N/A	N/A	N/A	N/A	N/A	N/A
9	Moderate	N	Y	Moderate	N	N	N/A	N/A	N/A	N/A	N/A	N/A
10	Moderate	N	N	Moderate to severe	N	N	N/A	N/A	N/A	N/A	N/A	N/A
11	Moderate to severe	N	N	Moderate to severe	Focal	N	N/A	N/A	N/A	N/A	N/A	N/A
12	Moderate to severe	N	N	Moderate	N	N	Y	N	Y	N/A	N/A	N/A
13	Mild to moderate	N	N	Mild	N	N	N/A	N/A	N/A	N/A	N/A	N/A
14	Severe	Multiple focal	N	Moderate	Diffuse	N	N/A	N/A	N/A	N/A	N/A	N/A
15	Mild to moderate	N	N	Moderate to severe	N	N	N/A	N/A	N/A	N/A	N/A	N/A
16	Severe	Multiple focal	N	Moderate to severe	N	N	N/A	N/A	N/A	N/A	N/A	N/A
17	Moderate	N	N	Moderate	N	N	N/A	N/A	N/A	N/A	N/A	N/A
18	Moderate	N	N	Mild	N	N	N/A	N/A	N/A	N/A	N/A	N/A
19	Mild	N	N	Moderate to severe	N	N	N/A	N/A	N/A	N/A	N/A	N/A
20	Moderate to severe	N	N	Moderate	N	N	Y	N	N	N	N	N
21	Mild	N	N	Moderate to severe	N	N	N	Y	Y	Y	N	N
22	Moderate	N	N	Mild to moderate	N	N	Y	N	N	N	N	Y
23	Moderate	N	N	Moderate	N	N	N	N	N	N	N	Y
24	Mild	N	N	Mild	N	N	N/A	N/A	N/A	N	N	N
25	Moderate to severe	N	N	Moderate to severe	N	N	Y	Y	Y	N	Y	Y
26	Mild to moderate	N	N	Mild	N	N	N/A	N/A	N/A	N/A	N/A	N/A

ATI, acute tubular injury; COVID-19, coronavirus disease 2019; EM, electron microscopy; FSGS, focal segmental glomerulosclerosis; ID, identification number; IF, immunofluorescent (stain); LM, light microscopy; N, not detected; N/A, not available; NP, nucleoprotein; SARS-CoV, severe acute respirator syndrome coronavirus; Y, detected.

both belong to the β-coronavirus family and utilize the same cellular receptor ACE2 for their entrance to target cells.[7,8] The renin angiotensin system plays essential roles in renal diseases via ACE-mediated angiotensin I to angiotensin II conversion. In addition, ACE2, discovered in 2000, negatively regulates the classic ACE–angiotensin II type 1 receptor axis.[9] In the kidneys, ACE2 is expressed in the apical brush borders of the proximal tubules as well as the podocytes in less intensity. In endothelial cells of the kidney, only ACE is expressed without detectable ACE2.[10,11] In line with this distribution of ACE2, we observed virus particles in tubular epithelium and podocytes, sites of known ACE2 expression. Collectively, the tubular and glomerular visceral epithelial cells of the kidney are the main targets of SARS-CoV-2. Based on our observations, the endothelium thus is not expected to be directly infected with SARS-CoV-2. However, we cannot totally rule out the possibility that SARS-CoV-2 can infect other resident kidney cells, as ACE2 expression may be altered in disease states or due to medications. Indeed, we show intensely positive parietal epithelial cells and occasional podocyte staining with ACE2 in 3 of the 5 COVID-19 kidney samples we assessed.

Recently, SARS-CoV-2 was shown to also invade target cells by CD147, a ubiquitously expressed transmembrane glycoprotein with interaction with diverse partners such as cyclophilins, caveolin-1, and integrins.[12] CD147 is thought to play a role in several kidney diseases through immune-inflammatory responses and dysregulated cell cycle. In the kidney, CD147 is highly expressed on the cell surface of proximal tubular epithelium and infiltrating inflammatory cells. Interestingly, the CD147 partners, cyclophilins, play an important role in the replication process of coronavirus, and cyclophilins' inhibitor, cyclosporine, can effectively suppress the intracellular propagation of virus.[13,14] Presumably, interrupting the CD147-cyclophilins axis may be a promising strategy to treat COVID-19.

In addition to the direct virulence of SARS-CoV-2, other secondary insults, especially hypoxia, cytokine storms, secondary infection with bacteria, other viruses, fungi, and drug-associated nephrotoxicity can all contribute to AKI.

In summary, we describe extensive ATI and a surprising endothelial injury pattern, with evidence for direct parenchymal tubular epithelial and podocyte viral infection in severe lethal COVID-19. However, there are several weaknesses

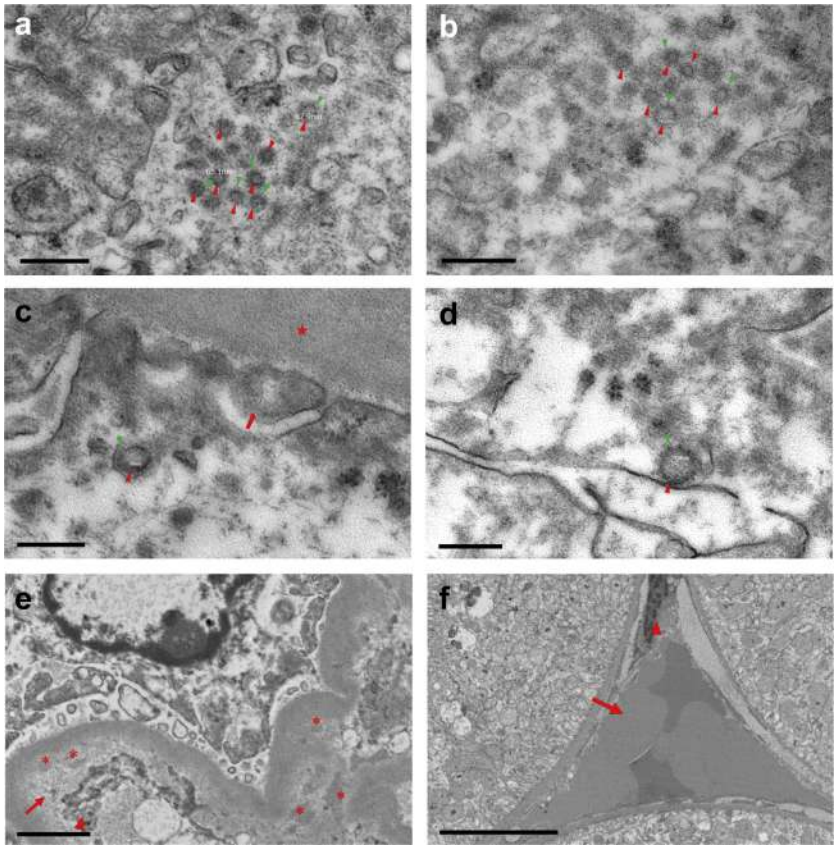

Figure 2| Ultrastructural features of kidneys from postmortems of patients with coronavirus disease 2019. (**a–d**) Virus particles (red arrowheads) with distinctive spikes (green arrowheads) were present in the cytoplasm of (**a**) the proximal and (**b**) distal tubular epithelium. (**c,d**) Virus particles (red arrowheads) with distinctive spikes (green arrowheads) were present in podocytes; foot processes of podocytes (arrow); glomerular basement membrane (star). (**e**) A single case of IgA nephropathy was diagnosed by immunofluorescent staining with a few paramesangial and subendothelial electron-dense deposits (asterisks) with marked subendothelial lucent expansion (arrow) and mesangial interposition (arrowhead). (**f**) Peritubular capillary with stasis of red blood cells (arrow) and activation or injury of endothelial cells (arrowhead). Transmission electron microscopy. Bars = (**a–d**) 200 nm, (**e**) 1 μm, and (**f**) 5 μm. To optimize viewing of this image, please see the online version of this article at www.kidney-international.org.

in the current study, including the relatively small number of cases, and the lack of control tissue from patients with less severe COVID-19 with evidence of AKI. Further research is still urgently needed for comprehensive understanding of COVID-19, including effects on the kidney.

METHODS

Patients

This study was conducted in accordance with the principles of the Declaration of Helsinki and approved by the Medical Ethical Committee of Union Hospital, Tongji Medical School, Huazhong University of Science and Technology. Written informed consent was obtained from next of kin of each enrolled case. According to the New Coronavirus Pneumonia Prevention and Control Program (7th edition), the diagnosis of COVID-19 was confirmed by nucleic acid testing of nasopharyngeal secretion or bronchoalveolar lavage fluids, radiologic features of viral pneumonia, and clinical symptoms. In addition, 5 patients also underwent assessment of the serum for SARS-CoV-2–specific antibodies detection by the immune colloidal gold technique, and all of them were positive.

Tissue sampling and processing

Samples from the kidney were obtained from autopsies of 26 COVID-19 cases with a postmortem interval ranging from 1 to 6 hours from February 18 to March 27, 2020. Tissue specimens were fixed in 10% formalin or 2.5% glutaraldehyde for 48 to 72 hours before the following procedures. Hematoxylin and eosin, periodic acid–Schiff, Masson trichrome, and Jones methenamine silver stains were performed on sections from paraffin blocks in all cases.

For EM examination, performed in 9 cases, after osmium tetroxide post fixation and gradient dehydration, Epon-embedded, toluidine blue-stained "semi-thin" sections were examined, and selected areas were chosen for thin sections. Thin sections were then cut and stained with uranyl acetate and lead citrate. EM grids were then viewed with a transmission electron microscope (HT-7800; Hitachi, Tokyo, Japan).

Immunohistochemical staining was performed in 9 to 16 cases for CD3, CD4, CD8, CD20, CD21, CD31, CD61, CD68, and CD235a (antibody source: Fuzhou Maixin Biotech Co., Ltd., Gulou Fuzhou, China). To detect the distribution of ACE2 in kidney, immunohistochemical staining was carried out, using antibody ACE2 from Abcam (catalog no. ab15348; Cambridge, MA). ACE2 staining was

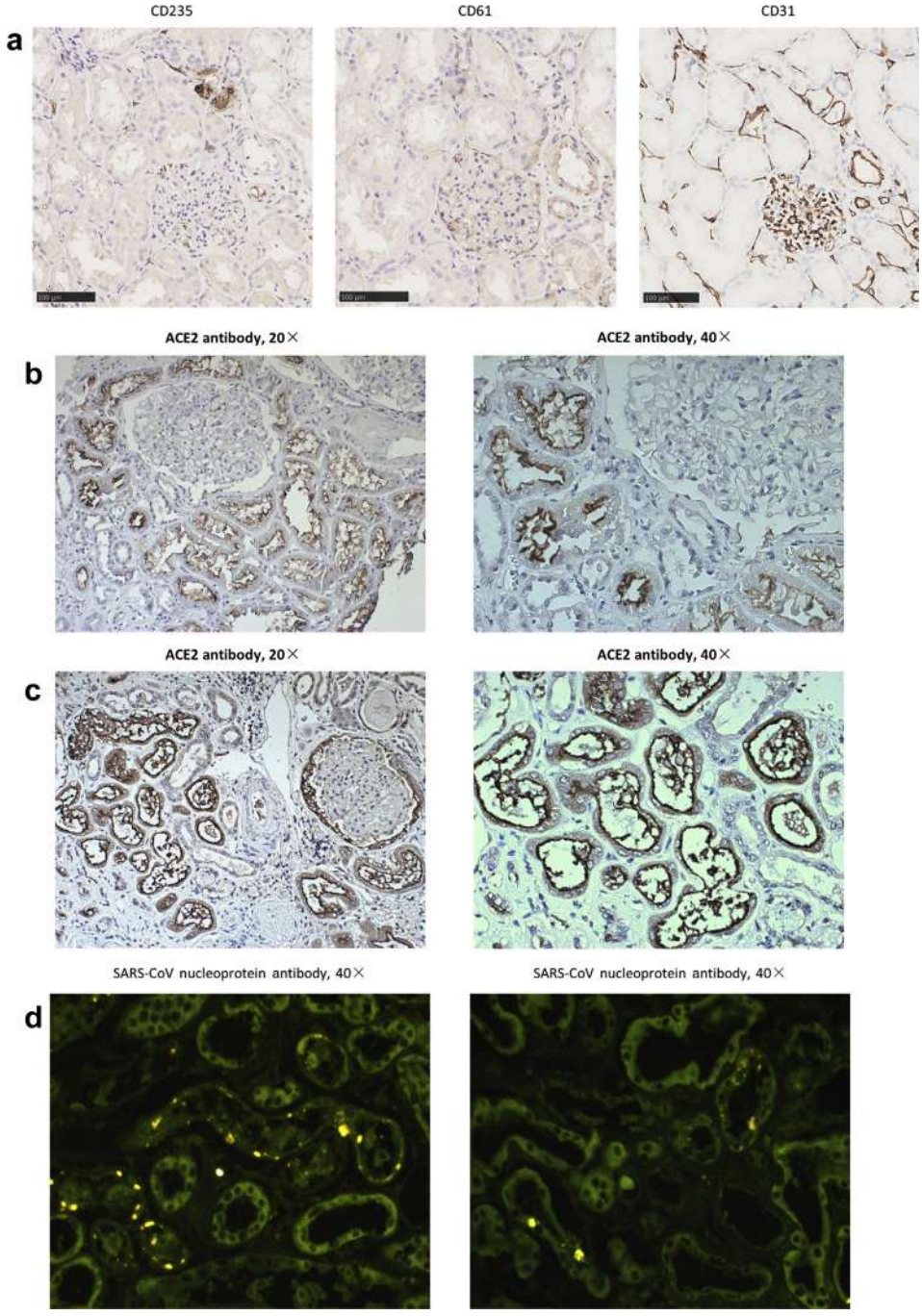

Figure 3 | Immunostaining of paraffin-embedded kidney tissue from patients with coronavirus disease 2019 (COVID-19). (**a**) Serial sections stained for CD235, CD61, and CD31 showing stasis of red blood cells without platelets in peritubular capillaries. Bars = 100 μm. (**b,c**) Angiotensin-converting enzyme II (ACE2) stained mainly proximal tubules in (**b**) non–coronavirus disease 2019 case, with (**c**) strong proximal tubular staining and parietal epithelial cell staining with occasional weak podocyte staining in some COVID-2019 cases. (**d**) Indirect immunofluorescent staining with anti–severe acute respirator syndrome coronavirus (SARS-CoV) nucleoprotein antibody. To optimize viewing of this image, please see the online version of this article at www.kidney-international.org.

performed in 5 COVID-19 cases and in an archival paraffin block from a patient without COVID-19, diabetes, or hypertension, who was biopsied for proteinuria.

IF staining was done in 6 cases for IgG, IgG subclasses, IgA, IgM, C3, C1q, kappa, and lambda by paraffin IF technique. Paraffin blocks from these 6 cases were also stained with anti-SARS-CoV nucleoprotein antibody (1:1000, 40143-T62; Sino Biological, Beijing, China) for 30 minutes in room temperature, and then stained with fluorescent-labeled secondary antibody.

DISCLOSURE

All the authors declared no competing interests.

ACKNOWLEDGMENTS

This work was financially supported by the International (Regional) Cooperation and Exchange Project (81961138007), the Key Special Project of Ministry of Science and Technology, China (grants 2020YFC0845700 and 2020YFC0845800), the National Natural Science Foundation of China (grants 81873602, 81570671, 81770711, and 81974096), the Fundamental Research Funds for the Central Universities (grant 2020kfyXGYJ101), Program for HUST Academic Frontier Youth Team (grant 2017QYTD20), and Hubei Provincial Natural Science Foundation of China (grant 2017CKB899).

REFERENCES

1. Lu R, Zhao X, Li J, et al. Genomic characterisation and epidemiology of 2019 novel coronavirus: implications for virus origins and receptor binding. *Lancet*. 2020;395:565–574.
2. Guan WJ, Ni ZY, Hu Y, et al. Clinical characteristics of coronavirus disease 2019 in China [e-pub ahead of print]. *N Engl J Med*. doi:10.1056/NEJMoa2002032. Accessed March 28, 2020.
3. Alsaad KO, Hajeer AH, Al Balwi M, et al. Histopathology of Middle East respiratory syndrome coronavirus (MERS-CoV) infection—clinicopathological and ultrastructural study. *Histopathology*. 2018;72:516–524.
4. Xu Z, Shi L, Wang Y, et al. Pathological findings of COVID-19 associated with acute respiratory distress syndrome. *Lancet Respir Med*. 2020;8:420–422.
5. Tietäväinen J, Mantula P, Outinen T, et al. Glucosuria predicts the severity of Puumala hantavirus infection. *Kidney Int Rep*. 2019;4:1296–1303.
6. Falk RJ, Jennette JC. ANCA small-vessel vasculitis. *J Am Soc Nephrol*. 1997;8:314–322.
7. Zhou P, Yang XL, Wang XG, et al. A pneumonia outbreak associated with a new coronavirus of probable bat origin. *Nature*. 2020;579:270–273.
8. Luan J, Lu Y, Jin X, Zhang L. Spike protein recognition of mammalian ACE2 predicts the host range and an optimized ACE2 for SARS-CoV-2 infection [e-pub ahead of print]. *Biochem Biophys Res Commun*. doi:10.1016/j.bbrc.2020.03.047. Accessed March 28, 2020.
9. Santos RAS, Sampaio WO, Alzamora AC, et al. The ACE2/angiotensin-(1-7)/MAS axis of the renin-angiotensin system: focus on angiotensin-(1-7). *Physiol Rev*. 2018;98:505–553.
10. Mizuiri S, Ohashi Y. ACE and ACE2 in kidney disease. *World J Nephrol*. 2015;4:74–82.
11. Lee SH, Lee YH, Jung SW, et al. Sex-related differences in the intratubular renin-angiotensin system in two-kidney, one-clip hypertensive rats. *Am J Physiol Renal Physiol*. 2019;317:F670–F682.
12. Wang K, Chen W, Zhou YS, et al. SARS-CoV-2 invades host cells via a novel route: CD147-spike protein. *bioRxiv*. doi:10.1101/2020.03.14.988345. Accessed March 28, 2020.
13. Tanaka Y, Sato Y, Sasaki T. Suppression of coronavirus replication by cyclophilin inhibitors. *Viruses*. 2013;5:1250–1260.
14. de Wilde AH, Raj VS, Oudshoorn D, et al. MERS-coronavirus replication induces severe in vitro cytopathology and is strongly inhibited by cyclosporin A or interferon-α treatment. *J Gen Virol*. 2013;94:1749–1760.